Studies of high-pressure *n*-butane oxidation with CO_2 dilution up to 100 atm using a supercritical-pressure jet-stirred reactor

Hao Zhao [a,b,*], Chao Yan [a], Tianhan Zhang [a], Guoming Ma [a], Michael J. Souza [c], Chong-wen Zhou [d], Yiguang Ju [a]

[a] *Department of Mechanical and Aerospace Engineering, Princeton University, Princeton, NJ 08544-5263, USA*
[b] *Department of Mechanical Engineering, The Hong Kong Polytechnic University, Hong Kong*
[c] *Department of Physics, Princeton University, Princeton, NJ 08544-5263, USA*
[d] *School of Energy and Power Engineering, Beihang University, Beijing, 100191, China*

Abstract

A novel supercritical-pressure jet stirred reactor (SP-JSR) is developed to operate up to 200 atm. The SP-JSR provides a unique platform to conduct kinetic studies at low and intermediate temperatures at extreme pressures under uniform temperature distribution and a short flow residence time. *n*-Butane oxidations with varying levels of CO_2 dilutions at pressures of 10 and 100 atm and over a temperature range of 500-900 K were conducted using the SP-JSR. The experiment showed that at 100 atm, a weak NTC behavior is observed and the intermediate temperature oxidation is shifted to lower temperatures. Furthermore, the results showed that CO_2 addition at supercritical conditions slows down the fuel oxidation at intermediate temperature while has little effect on the low temperature oxidation. The Healy model under-predicts the NTC behavior and shows little sensitivity of the effect of CO_2 addition on the n-butane oxidation. Reaction pathway and sensitivity analyses exhibit that both the low and intermediate temperature chemistries are controlled by RO_2 consumption pathways. In addition, the reactions of $CH_3CO (+ M)$ and $CH_3CO + O_2$ become important at 100 atm. The results also revealed that fuel oxidation kinetics is insensitive to the third body effect of CO_2. The kinetic effect of supercritical CO_2 addition may come from the reactions involving H_2O_2, CO, CH_2O, and CH_3CHO, especially for the reactions of $CO_2 + H$ and $CO_2 + OH$.

* Corresponding author at: Department of Mechanical and Aerospace Engineering, Princeton University, Princeton, NJ 08544-5263, USA; Department of Mechanical Engineering, The Hong Kong Polytechnic University, Hong Kong.

E-mail address: cgsq725525@gmail.com (H. Zhao).

1. Introduction

Supercritical combustion has increasingly gained attention for its high thermodynamic efficiency, low pollutant emissions, and applications in advanced internal combustion engines, gas turbines, and air-breathing engines, in which the

operating pressure reaches up to several hundreds of atmospheres [1–4]. However, at such high pressure and temperature conditions, the gas-phase kinetic theory needs to be re-evaluated due to the real-fluid effects, including the non-plastic collision effect and the multiple collision effect, and the properties of substance, transports, and molecules might be different due to the failure of Boltzmann assumption. As a result, reaction rates, even for some well calculated or measured reactions like $CO + OH = CO_2 + H$, $H + O_2 + M = HO_2 + M$, and $H + O_2 = OH + O$, might have a significant discrepancy between supercritical and gas-phase conditions. As such, kinetic experiments and theoretical calculations at ultra-high pressures (above 100 atm) are necessary for understanding supercritical combustion chemistry.

Shao et al. [5] measured ignition delay times of methane and hydrogen highly diluted in carbon dioxide at 300 atm and studied the effect of supercritical CO_2 on the fuel ignition. Kogekar et al. [6] studied the impact of non-ideal behavior on ignition delay time of n-dodecane in high-pressure shock tube. Liang et al. [3] evaluated the effects of properties of thermodynamics and transports on hydrogen and methane flame speed measurements at supercritical conditions, and it was found that the laminar flame speeds at high pressures increase due to the non-ideal equation of state. Hashemi et al. [7–9] used a high-pressure laminar flow reactor to study the supercritical oxidation chemistries of methane, ethane, and propane at 100 atm and built high pressure models. Fernandes et al. [10] used a high-pressure flow reactor to perform elementary reaction rate measurements up to 1000 bar. Unfortunately, only a few research apparatuses in the field of combustion such as the shock tube [5,6] and high pressure laminar flow reactor [7–9,10] can be used to study supercritical reaction chemistry. The shock tube has challenges in flow residence time (10-20 ms) and is mainly used for high temperature ignition study with a small scale of speciation. As to the laminar flow reactor [7–9], at first, the residence time is very long (above 10 s) so that the fuel concentration has to be very low to slow down the reactivity. Therefore, this laminar reactor did not show any NTC effect even for propane oxidation at 100 atm. Second, the temperature in the laminar flow reactor is not uniform (3 sections with 300 K deviation), therefore, neither the temperature nor the reactor flow residence time is well-defined. Due to these problems, a new research apparatus for supercritical kinetics study is highly necessary.

The jet-stirred reactor (JSR) has been widely used as a chemical reactor for the development and validation of detailed chemical mechanisms of fuels [11–13]. A toroidal reactor was proposed by Nenniger [14], in which multiple jets were distributed on the outside sidewall of the JSR. An outward cross-injector (OCI) JSR was developed by Dagaut [15], which is widely used in the last 30

years. However, there exists large non-uniformities in terms of temperature, flow velocity, and residence time distributions inside these two types of JSRs, thereby limiting their utility as ideal JSRs [16]. This paper presents a novel supercritical-pressure jet stirred reactor (SP-JSR), which shows the following unique properties. (1) The first JSR which can operate between 10–200 atm and 300-1200 K to study supercritical CO_2 and water effects. (2) A well-defined flow residence time between 0.1–1 second (more engine relevant conditions) and a uniform temperature distribution within 5 K deviation. (3) The first flow system capturing the NTC behavior clearly at 100 atm. (4) It provides complimentary and cross-validation data for other experiments. The geometrical design of the SP-JSR has been published in artical [17], which is available among the supplementary materials.

In addition, *n*-butane, as a major component of liquefied petroleum gas and simple alkane with rich low temperature chemistry [18–20], has been extensive investigated in shock tubes [20–23], spherical flames [24–26], flow reactor [27], JSR [28–30], and rapid compression machines (RCM) [31,32]. However, the performances of recently developed models of Healy [20], Li et al. [26], and Bahrini et al. [30] are distinctly different, especially at low temperatures. Moreover, the speciation experiments in flow reactor and JSR in literatures were only conducted at pressures lower than 10 atm, while higher pressure experimental data are needed close to engine conditions.

To study the oxidation chemistry of *n*-butane at supercritical conditions and extend the available data toward engine conditions, this paper presents the experimental and modeling results of *n*-butane oxidation with and without 20% CO_2 additions at pressures of 10 and 100 atm and temperature of 500–900 K by using the novel SP-JSR. The mole fractions of n-C_4H_{10}, O_2, CO, CO_2, CH_2O, C_2H_4, CH_3CHO, C_3H_6, and C_4H_8 are quantified by using a micro-gas chromatograph (μ-GC). Moreover, the effect of supercritical CO_2 on the oxidation is also investigated by adding 20% CO_2 to the reactant mixture at 100 atm. Then, the high-pressure, low and high temperature chemistry of *n*-butane is analyzed and a chemical kinetic model of *n*-butane is evaluated and updated with identification of key reactions.

2. Experimental methods and kinetic models

2.1. Geometry of the SP-JSR

As is shown in Fig. 1 [17], the SP-JSR is a sphere with an internal volume of 0.5 cm^3. Compared to the OCI JSR design in [15], the novelty of the SP-JSR is its 8 nozzles with 0.2 mm inner diameter on 4 jet fingers at the center of the sphere, which generate intense turbulence and homogenous mixing.

Fig. 1. The quartz supercritical-pressure jet stirred reactor [17].

The eight nozzles are placed in such a way that net vertex is avoided and residence time of the flow is closer to the corresponding theoretical value than previous 4 jet designs. This ensures homogeneity in concentration and residence time distributions inside the reactor. The SP-JSR design also passes the four criteria of JSR design [11]. The schematic of the SP-JSR jet geometry is shown in Figure S1 (a) and more details are available in the supplementary document. Furthermore, numerical simulations using ANSYS 14.0-CFX are conducted for comparing the performance of the SP-JSR and traditional OCI JSR [15]. The velocity distributions, the spatial cuts through the velocity field, and the mean flow residence time calculations for the SP-JSR and the OCI JSR are plotted in Figure S1 (b)-(d), respectively, at 800 K and 10 atm with fixed jet velocity of 40 m/s in a CH_4/air mixture. It can be seen that in the OCI JSR, net turbulence vertex is formed in the flow field, resulting in non-uniformity in velocity, temperature, and species. However, in the present SP-JSR, there is no observation of significant vertex, and a better homogeneity with smaller deviations of the mean flow residence time is achieved in the SP-JSR than the previous one.

2.2. Experimental setup and validation

The quartz reactor is placed inside a stainless-steel pressure-resistant jacket. By means of pressure balancing inside and outside the reactor, the high pressure working condition is possible. The gases issuing from the JSR exit are sampled by a quartz sonic nozzle, and then equilibrate their pressure with vacuum generated by a dry pump. The experimental system was designed for experiments over 1–200 atm and 298 – 1050 K temperature range. The schematic of the setup is shown in Fig. 2, and the detailed description is in the supplementary document. The gas flow rates were

controlled by high-pressure mass flow controllers (Brooks, SLA5800) and gas samples were quantified by using a micro gas chromatograph (μ-GC) [33,34].The axial temperature profiles under the experimental flow conditions were measured in 1 mm steps along the JSR bulb, where the temperature variation is within $\pm$ 3 K between 400-1000 K. The temperature profile is plotted in Figure S2 in the supplementary document.

Propane is the simplest alkane showing low temperature chemistry. Healy et al. [35] studied propane low and high temperature chemistry at elevated pressures in shock tube and RCM in 2008, and the model of propane oxidation has been updated and validated in AramcoMech 3.0 framework [36]. We performed the propane oxidation at 10 atm in the SP-JSR and used the propane model in the well-developed AramcoMech framework to validate the experimental measurements made by the SP-JSR. The experimental and modeling results of propane oxidation at 10 atm are plotted in Figure S3 (a) in the supplementary document. The model prediction and experimental data agree with each other very well. It is noted that NTC behavior is not observed in the propane oxidation at 10 atm in this experiment. DME is another simple molecule, which shows a stronger low temperature chemistry than propane. Therefore, we further performed the experiment of DME oxidation at 10 atm in the SP-JSR and the Chemkin simulation by using the HP DME model [37] to specify the NTC behavior for the SP-JSR validation (Figure S3 (b)). It shows that the NTC behavior of DME at 10 atm is well captured by the SP-JSR.

The experiments were performed between 500-900 K at pressures of 10 and 100 atm with and without 20% CO_2 additions in the three cases in Table 1. The inlet volume flow rate was fixed at 0.6 and 6 L/min at 1 atm and 293 K for case 1 and cases 2 and 3, respectively; as such, the residence time in the reactor varies with temperature (Table 1).

2.3. Modeling details

Kinetic models of Healy [20], Li et al. [26], and Bahrini et al. [30] have been used in the present study. We use Healy's model [20] as the base model in the main content. The model simulations by using the other two mechanisms are added in the supplementary document in Figure S4 as a reference. Reaction rates of n-C_4H_{10} + HO_2, C_2H_5 + HO_2, C_4H_8OOH + O_2, CH_3CO + O_2, and H_2O_2 (+ M) in Healy's model are updated within their rate uncertainties in this study, and are listed in Table S2 in the supplementary document.

3. Results and discussion

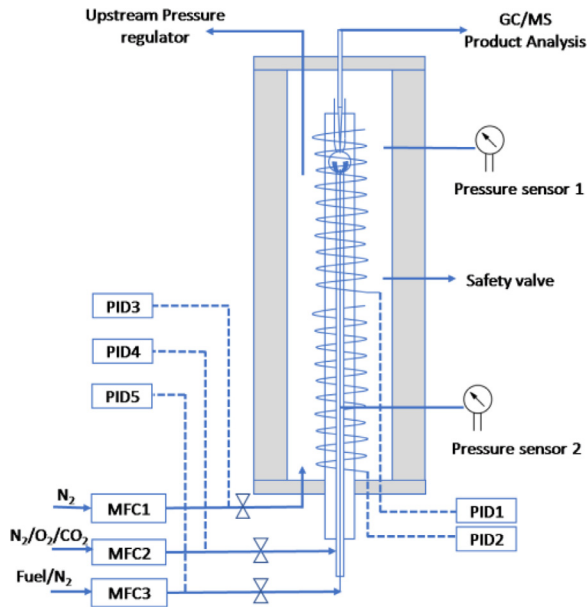Fig. 3 depicts the mole fraction of n-C_4H_{10} against temperature with and without 20% CO_2

Fig. 2. Schematic of the SP-JSR setup.

Table 1
Experimental conditions.

Case	Equivalence ratio	Pressure (atm)	n-C$_4$H$_{10}$ (%)	O$_2$ (%)	N$_2$ (%)	CO$_2$(%)	Residence time (s)	Temperature (K)
1	0.1	10	0.2	13	86.8	0	0.234–0.13	500–900
2	0.1	100	0.2	13	86.8	0	0.234–0.13	500–1000
3	0.1	100	0.2	13	66.8	20	0.234–0.13	500–1000

additions at 10 and 100 atm. Experimental data shows a typical low temperature window from 600 K to 780 K and a clear negative temperature coefficient (NTC) behavior at 10 atm without CO$_2$ addition (case 1), while a weak NTC behavior is observed and the intermediate temperature oxidation is shifted to lower temperatures at 100 atm with (case 3) and without (case 2) CO$_2$ additions. The onset temperature of low temperature oxidation changes insignificantly with pressure. From the experimental data in cases 2 and 3, it is seen that supercritical CO$_2$ has limited effect on the low temperature oxidation of n-butane, while slows down the intermediate temperature oxidation. This observation agrees with previous literature [38–40]. n-Butane is completely consumed at around 800 K without CO$_2$ addition, and it is delayed to 850 K with 20% CO$_2$ addition. Healy's model predicts the onset of the low temperature oxidation of n-butane well for all three cases. However, it under-predicts the NTC behavior and the intermediate temperature oxidation, and the discrepancy becomes larger at a higher pressure. Furthermore, the model simulation shows little difference between the experiments with and without 20% CO$_2$ additions at 100 atm. It implies that Healy's model is not sensitive

to the effect of CO$_2$ addition on the n-butane oxidation. The updated model will be discussed later.

To explain the effect of pressure on the n-butane oxidation, a pathway analysis of n-butane is performed at 100 and 10 atm at 740 K for case 2 in Fig. 4(a) and (b), respectively. The schematics of reaction pathways at lower and higher temperatures and with 20% CO$_2$ addition are similar to those in Fig. 4 and are not plotted here. In Fig. 4(a), the two important radicals of s-C$_4$H$_9$ and p-C$_4$H$_9$, noted as R, are formed from H abstraction reactions of n-butane by OH and HO$_2$ radicals and further produces RO$_2$ (C$_4$H$_9$O$_2$) through the first O$_2$ addition. It is well-known that the reaction pathways shown in black of Fig. 4 dominate the low temperature chemistry of alkanes at lower pressures, and the QOOH (C$_4$H$_8$OOH) competing reactions of QOOH + O$_2$ = O$_2$QOOH (R$_1$) and QOOH = QO + OH (R$_2$) control the NTC behavior. The reaction of RO$_2$ = QOOH (R$_3$) is the main reaction to form QOOH. However, at higher pressures up to 100 atm, R$_1$ becomes much more important than R$_2$ due to the intense collision between QOOH and O$_2$ and fast relaxation of excited O$_2$QOOH. As a result, R$_1$ dominates the n-butane oxidation at a broader temperature range
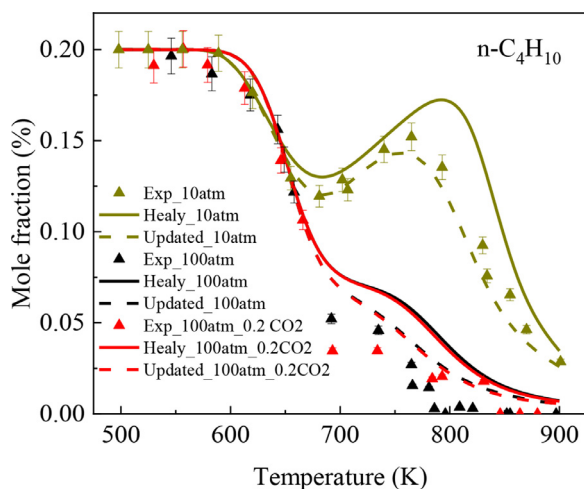
Fig. 3. Temperature evolution of the fuel mole fraction, n-C_4H_{10}, from 500 to 900 K with and without CO_2 additions, at 10 and 100 atm, and by using Healy's and the updated models, respectively.

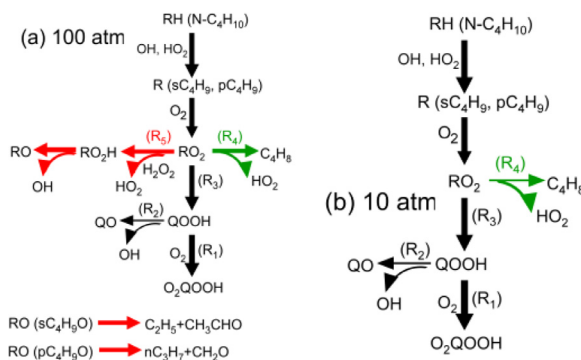Fig. 4. Reaction pathways for *n*-butane without CO_2 addition at 100 atm (a) and 10 atm (b) at 740 K by using Healy's model. The thickness of arrows here represents the relative importance of different reaction pathways based on the rate of species production.

and the NTC behavior is reduced at 100 atm. On the other hand, the reaction of $RO_2 = HO_2 + C_4H_8$ (R_4), which is the main reaction channel at intermediate temperature (800-1000 K), appears in the NTC region. It indicates that the intermediate temperature chemistry is shifted to the NTC region at 100 atm, and the boundary between low and intermediate temperature chemistries becomes indistinct. Moreover, due to the larger pool of HO_2 and H_2O_2 at 100 atm, $RO_2 + H_2O_2 = RO_2H + HO_2$ (R_5) appears in the RO_2 pathways. At 10 atm in Fig. 4(b), reaction channel R_4 is not important at 740 K and R_5 does not show up, which agrees with the discussion above. In summary, a weak NTC behavior is observed at 100 atm. Both the low and intermediate temperature chemistries are controlled by RO_2 reaction pathways through R_3-R_5. This also explains why the reaction pathways at lower and higher temperatures at 100 atm are similar.

Furthermore, to investigate the discrepancy between experiment and model simulation in the NTC and intermediate temperature region, the sensitivity analyses of *n*-butane without CO_2 addition at a pressure of 100 atm and temperatures of 740 and 800 K are plotted in Fig. 5(a) and (b), respectively. It is seen in Fig. 5(a) and (b) that *n*-butane oxidation is largely controlled by H-abstraction from *n*-butane by OH, RO_2 competing reactions by R_3 and R_4, and CH_2O/HCO chemistry. Moreover, reactions in the H_2O_2/HO_2 chemistry, which are generally important in the intermediate temperature region [37], are also sensitive at 740 K in the NTC region. Therefore, it confirms the statement in the pathway analysis that the intermediate temperature chemistry is shifted to lower temperature in the NTC region at 100 atm. In addition, comparing the sensitivity analyses of *n*-butane at 100 atm in Fig. 5(a) and the at 10 atm in Figure S5 at 740 K, it
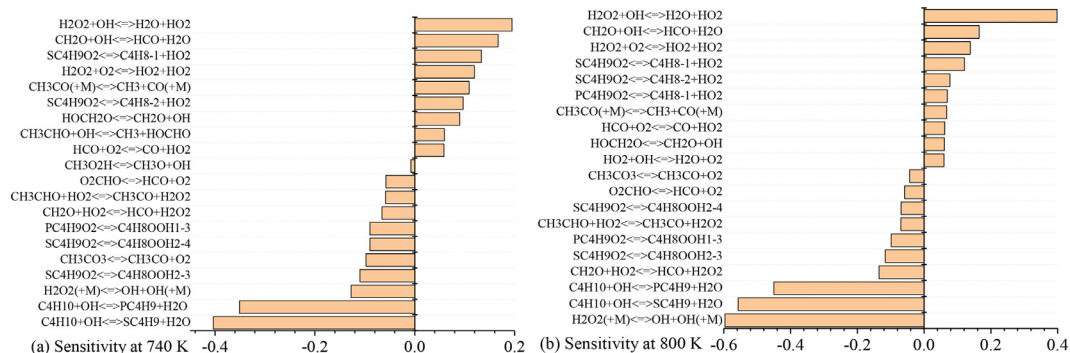
Fig. 5. Sensitivity analyses for *n*-butane without CO_2 addition at 740 (a) and 800 K (b) and at 100 atm by using Healy's model.

is seen that R_4 at 100 atm is more important than that at 10 atm, which is corresponding with the statement in the pathway analysis above. Moreover, it is interesting to note that the competing reactions of $CH_3CO (+ M)$ and $CH_3CO + O_2$ show up at 100 atm, while are not important at 10 atm. Theoretical calculations and measurements for these reaction rates need to be emphasized for the high pressure chemistry model development.

Based on the pathway and sensitivity analyses and the present high pressure experimental data, Healy's model is updated with modifying reaction rates of R_1, $CH_3CO + O_2$, and $H_2O_2 (+ M)$ within uncertainties of calculations or measurements. It is seen in Fig. 3 that the updated model has a better prediction of the experimental data, especially in the NTC and intermediate temperature region. However, the model still slightly under-predicts the *n*-butane oxidation and cannot capture the effect of supercritical CO_2 on the oxidation. The sensitivity analysis of CO_2 for case 3 at 800 K, which is depicted in Figure S6 in the supplementary document, shows that reactions of $CO + OH = CO_2 + H$, $H_2O_2 (+ M) = 2OH (+ M)$, $CH_2O + OH = HCO + H_2O$, and $CH_3CO (+ M) = CH_3 + CO (+ M)$ are the most sensitive reactions. There are mainly three influences of CO_2 addition on the *n*-butane oxidation. (1) CO_2 enhances the third body collision efficiencies in comparison to N_2. We have perturbed the collision efficiency of CO_2 in the four main third body reactions, $H_2O_2 (+ M) = 2OH (+ M)$, $CH_3CO (+ M) = CH_3 + CO (+ M)$, $HCO (+ M) = H + CO (+ M)$, and $H + O_2 (+ M) = HO_2 (+ M)$, by factor of two, however, the simulation still shows little difference between case 2 and 3. It implies that the influence of CO_2 collision efficiency might be negligible or there are missing important third body reactions at supercritical conditions. This observation corresponds with those in [38,39]. (2) CO_2 participates in chemical reactions in the

oxidation process, like $CO + OH = CO_2 + H$ and $CO + HO_2 = CO_2 + OH$. The former is the key exothermal reaction in the oxidation, and Joshi et al. [41] modeled its pressure dependence through the reactions of $CO + OH (+ M) = HOCO (+ M)$ and $HOCO = CO_2 + H$ at high pressures. It is interesting to note that the reaction of $CO + OH = CO_2 + H$ does not reach the high pressure limit at 100 atm according to Joshi's calculation. The latter becomes important due to the large production of HO_2 at high pressures and low and intermediate temperatures. Future work on the theoretical calculations and evaluations of these two reactions at supercritical conditions is needed for analyzing the effect of supercritical CO_2 on the fuel oxidation. (3) CO_2 has a higher heat capacity than N_2, and its thermal and transport properties are different at supercritical conditions [42]. Therefore, a model simulation considering the supercritical thermal and transport properties of reactants and products is required to analyze the CO_2 effect on the high pressure oxidation in the future work.

The mole fractions of other important products and intermediates, such as O_2, CO, CO_2, C_2H_4, CH_2O, and CH_3CHO, are plotted in Fig. 6(a)-(f), respectively. It is seen that the updated model improves the predictability for all the key species in Fig. 6 compared to the original model. It is clearly seen in Fig. 6(a)-(f) that the NTC behavior is suppressed at 100 atm and the low and intermediate temperature chemistry "merge" together, which corresponds with the pathway analysis in Fig. 4. Furthermore, the low and intermediate temperature peaks of C_2H_4, CH_2O, and CH_3CHO even merge to a single peak in Fig. 6(d)-(e), respectively. The deceleration effect of CO_2 addition at 100 atm is also observed in the mole fraction profiles of CO, CH_2O, and CH_3CHO in Fig. 6(b), (e), and (f), respectively. It implies that reactions involved in CO, (like $CO + OH = CO_2 + H$ and $CO + HO_2 = CO_2 + OH$), CH_2O (like
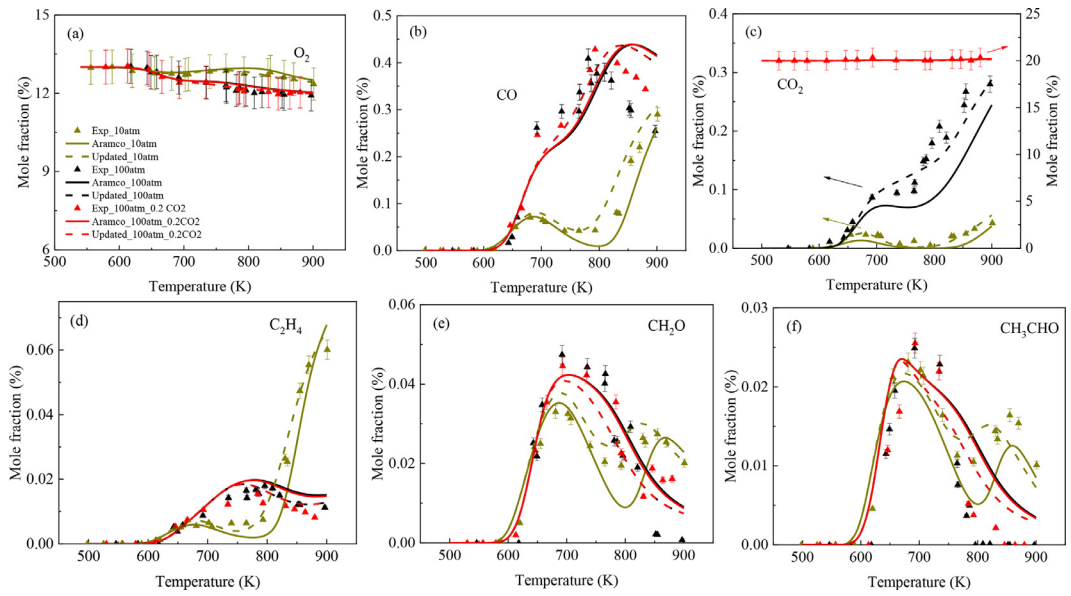
Fig. 6. Temperature evolutions of the mole fraction of O_2 (a), CO (b), CO_2 (c), C_2H_4 (d), CH_2O (e), and CH_3CHO (f) from 500 to 900 K with and without CO_2 additions, at 10 and 100 atm, and by using Healy's and the updated models, respectively.
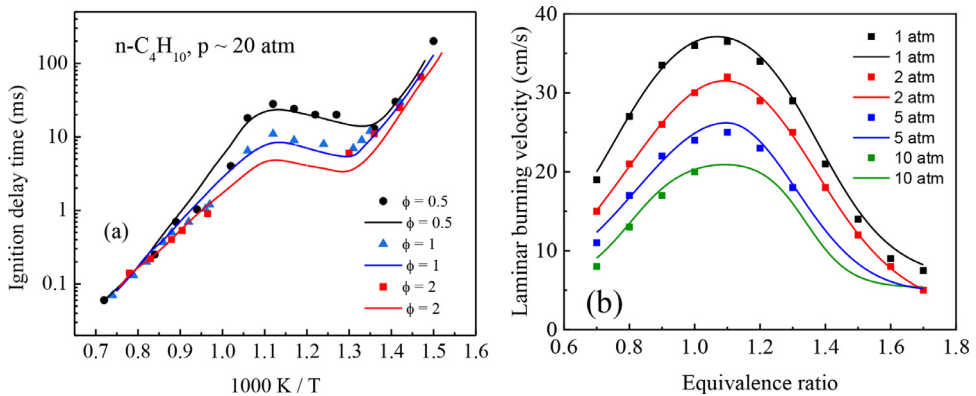

Fig. 7. (a) Ignition delay time of *n*-butane/air mixture with different equivalence ratios at 20 atm and (b) laminar burning velocity of *n*-butane/air mixture with different equivalence ratios at 1–10 atm in literature experiments and model simulations by using the updated model in this paper. Lines are model simulations. The ignition delay time data in (a) are from [20], while the flame speed data in (b) are from [26].

$CH_2O + OH = HCO + H_2O$), and CH_3CHO (like $CH_3CHO + OH = CH_3CO + H_2O$ and $CH_3CO (+ M) = CH_3 + CO (+ M)$) may explain the deceleration effect of supercritical CO_2 addition. It should be noted that the discrepancy between experiment and model simulation for CO production is still large at around 850 K. Therefore, the reactions of $CO_2 + H = CO + OH$ and $CO_2 + OH = CO + HO_2$ need careful evaluations at supercritical conditions. The supercritical

CO_2 effect on oxidation is complicated and is still not clear in literature. It requires future work on theoretical calculations on reaction rates at supercritical conditions, such as $CO_2 + H/OH$, and on the third-body collision factors of CO_2.

4. Comparison with literature data

The updated *n*-butane model is also validated against the ignition delay time data at 20 atm from

[20] in Fig. 7(a) and flame speed data at 1–10 atm from [26]. It is seen that the updated model predicts both the ignition delay time and the laminar flame speed well at different equivalence ratios and pressures.

5. Conclusion

This paper presents a novel supercritical-pressure jet stirred reactor (SP-JSR), which can operate up to 200 atm. The SP-JSR provides an unprecedented platform to conduct kinetic studies at low and intermediate temperatures at extreme pressures under uniform temperature distribution and a short flow residence time around 0.1 s.

The SP-JSR was used to study the *n*-butane oxidation with different levels of CO_2 additions at pressures of 10 and 100 atm and temperaturebetween500-900 K. The experiments show that a weak NTC behavior is observed at 100 atm and that the intermediate temperature oxidation is shifted to lower temperatures. Moreover, supercritical CO_2 decelerates the intermediate temperature oxidation. Healy's model under-predicts the NTC behavior and shows little sensitivity of the effect of CO_2 addition on the *n*-butane oxidation.

Pathway and sensitive analyses exhibit that both the low and intermediate temperature chemistries are controlled by RO_2 reaction pathways through the reactions of $RO_2 = QOOH$ (R$_3$), $RO_2 = HO_2 + C_4H_8$ (R$_4$), and $RO_2 + H_2O_2 = RO_2H + HO_2$ (R$_5$), in which R$_5$ appears due to the high level of HO_2/H_2O_2 content at high pressures. In addition, the competing reactions of CH_3CO (+ M) and $CH_3CO + O_2$ are important at 100 atm, while are not sensitive at lower pressures. Kinetic sensitivity analysis did not show the influence of the CO_2 third body effect at 100 atm. The effect of supercritical CO_2 addition on the oxidation may come from the reactions involving H_2O_2, CO, CH_2O, and CH_3CHO, especially, the reactions of $CO_2 + H = CO + OH$ and $CO_2 + OH = CO + HO_2$ need careful reevaluations at supercritical conditions. A kinetic model is updated and it improves the predictability of major products and intermediates.

Declaration of Competing Interest

None.

Acknowledgements

Supplementary materials

Supplementary material associated with this article can be found, in the online version, at doi:10.1016/j.proci.2020.08.047.

References

[1] R.D. Reitz, *Int. J. Engine Res.* 14 (2013) 411–415.
[2] G.P. Sutton, O. Biblarz, *Rocket Propulsion Elements*, John Wiley & Sons, 2016.
[3] W. Liang, W. Li, C.K. Law, *Proc. Combust. Inst* 37 (2019) 1733–1739.
[4] H. Zhao, N. Zhao, C. Yan, Z. Zhang, Y. Ju, *Combust. Flame* 212 (2020) 337–344.
[5] J. Shao, R. Choudhary, D.F. Davidson, R.K. Hanson, S. Barak, S. Vasu, *Proc. Combust. Inst.* 37 (2019) 4555–4562.
[6] G. Kogekar, C. Karakaya, G.J. Liskovich, M.A. Oehlschlaeger, S.C. DeCaluwe, R.J. Kee, *Combust. Flame* 189 (2018) 1–11.
[7] H. Hashemi, J.M. Christensen, S. Gersen, H. Levinsky, S.J. Klippenstein, P. Glarborg, *Combust. Flame* 172 (2016) 349–364.
[8] H. Hashemi, J.G. Jacobsen, C.T. Rasmussen, et al., *Combust. Flame* 182 (2017) 150–166.
[9] H. Hashemi, J.M. Christensen, L.B. Harding, S.J. Klippenstein, P. Glarborg, *Proc. Combust. Inst.* 37 (2019) 461–468.
[10] R.X. Fernandes, K. Luther, J. Troe, *J. Phys. Chem. A* 110 (2006) 4442–4449.
[11] R. David, D. Matras, *Can. J. Chem. Eng.* 53 (1975) 297–300.
[12] H. Zhao, A.G. Dana, Z. Zhang, W.H. Green, Y. Ju, *Energy* 165 (2018) 727–738.
[13] H. Zhao, L. Wu, C. Patrick, et al., *Combust. Flame* 197 (2018) 78–87.
[14] J. Nenniger, A. Kridiotis, J. Chomiak, J. Longwell, A. Sarofim, *Proc. Combust. Inst.* 20 (1985) 473–479.
[15] P. Dagaut, M. Cathonnet, J. Rouan, et al., *J. Phys. E. Sci. Instrum.* 19 (1986) 207.
[16] T. Zhang, H. Zhao, Y. Ju, *AIAA J* 56 (2018) 3388–3392.
[17] H. Zhao, M. Souza, Y. Ju, *Fusion: J. Am. Sci. Glassblowers Soc.* 66 (2018) 19–24.
[18] A. Demirbas, *Energy Sources* 24 (2002) 601–610.
[19] N. Donato, C. Aul, E. Petersen, C. Zinner, H. Curran, G. Bourque, *J. Eng. Gas Turb. Power* 132 (2010) 051502.
[20] D. Healy, N. Donato, C. Aul, et al., *Combust. Flame* 157 (2010) 1526–1539.
[21] X. Jiang, Y. Zhang, X. Man, L. Pan, Z. Huang, *Energ. Fuel.* 28 (2014) 2189–2198.
[22] D. Healy, N. Donato, C. Aul, et al., *Combust. Flame* 157 (2010) 1540–1551.
[23] X. Jiang, Y. Zhang, X. Man, L. Pan, Z. Huang, *Energ. Fuel.* 27 (2013) 6238–6246.
[24] O. Park, P.S. Veloo, D.A. Sheen, Y. Tao, F.N. Egolfopoulos, H. Wang, *Combust. Flame* 172 (2016) 136–152.
[25] H. Wu, E. Hu, H. Yu, et al., *Energ. Fuel* 28 (2014) 3412–3419.
[26] W. Li, G. Wang, Y. Li, et al., *Combust. Flame* 191 (2018) 126–141.

[27] S.D. Klotz, K. Brezinsky, I. Glassman, *Proc. Combust. Inst.* 27 (1998) 337–344.

[28] P. Dagaut, J. Luche, M. Cathonnet, *Energ. Fuel.* 14 (2000) 712–719.

[29] P. Dagaut, J. Luche, M. Cathonnet, *Int. J. Chem. Kinet.* 32 (2000) 365–377.

[30] C. Bahrini, P. Morajkar, C. Schoemaecker, et al., *Phys. Chem. Chem. Phys.* 15 (2013) 19686–19698.

[31] R. Minetti, M. Ribaucour, M. Carlier, C. Fittschen, L.R. Sochet, *Combust. Flame* 96 (1994) 201–211.

[32] S. Kojima, T. Suzuoki, *Combust. Flame* 92 (1993) 254–265.

[33] H. Zhao, J. Fu, F.M. Haas, Y. Ju, *Combust. Flame* 183 (2017) 253–260.

[34] Z. Zhang, H. Zhao, L. Cao, G. Li, Y. Ju, *Energ. Fuel* 32 (2018) 11970–11978.

[35] D. Healy, H. Curran, S. Dooley, et al., *Combust. Flame* 155 (2008) 451–461.

[36] C.W. Zhou, Y. Li, U. Burke, et al., *Combust. Flame* 197 (2018) 423–438.

[37] H. Zhao, X. Yang, Y. Ju, *Combust. Flame* 173 (2016) 187–194.

[38] B. Koroglu, O.M. Pryor, J. Lopez, L. Nash, S.S. Vasu, *Combust. Flame* 164 (2016) 152–163.

[39] J.W. Hargis, E.L. Petersen, *Energ. Fuel* 29 (2015) 7712–7726.

[40] T. Le Cong, P. Dagaut, *Proc. Combust. Inst.* 32 (2009) 427–435.

[41] A.V. Joshi, H. Wang, *Int. J. Chem. Kinet.* 38 (2006) 57–73.

[42] H. Zhao, Z. Zhang, Y. Rezgui, N. Zhao, Y. Ju, *Combust. Flame* 200 (2019) 135–141.